Use of High Resolution Space Imagery to Monitor the Abundance, Distribution, and Migration Patterns of Marine Mammal Populations

Ron Abileah, SRI International
333 Ravenswood Avenue
Menlo Park, CA 94025

***Abstract*—Aerial surveys are routinely used to study marine mammal populations. Recently, the resolution of imagery from commercial satellites has improved to the point where individual marine mammals can be detected. It may therefore be possible to perform remote sensing of marine mammal populations from space. This paper presents an initial assessment of detectability. A simple signal and noise model is developed to predict the signal-to-noise ratio (SNR) for a whale-like target. SNR is calculated for three cases: detection limited by sensor quantization noise ("best case"); detection in real noise, using one spectral band image; and detection in real noise, using a two-band noise reduction technique. An Ikonos satellite image was used for a realistic noise spectrum. The calculations show that a canonical target of length = 14 m and average spectral reflectivity can be detected up to depth of 24 m. Thus a case can be made for using satellites to monitor marine mammal abundance and geographical distributions, and to observe migratory patterns in remote areas.**

I. INTRODUCTION

Aerial surveys are effective for studying marine mammals, especially in habitats near shores. For example, Mobley et al. [1] used aerial surveys to map the geographical extent of the humpback whale's Hawaii wintering grounds, and repeat surveys from 1993 through 2000 documented a healthy recovery of the population. In addition, aerial surveillance is used to ensure compliance with the Marine Mammals Protection Act. The best-known example of such surveillance is the Early Warning System (EWS), a consortium of aerial surveys that monitors the location of the northern right whale population off the U.S. Atlantic coast. Animal locations are reported and then disseminated to maritime traffic. EWS has turned out to be a very successful effort to minimize ship strikes to this most endangered species. Another example is the use by Carretta et al. [2] of aerial surveys in around San Clement Island, California, to help the Navy assess the environmental impact of its operations in that area.

In a typical survey, a small aircraft and personnel are deployed to the survey area. Data is collected on linear flight transects. Two observers view the ocean surface through bubble windows in the belly of the aircraft, and their visual detections are recorded by a third individual. With a typical flying altitude of 300 m, an instantaneous field of view of 150 m, and an aircraft velocity of 50 m/s, the survey covers 27 km^2/hr. Operation times are limited by weather conditions, sun illumination, and sea state.

Now that several commercial high-resolution satellites (Table 1) are (or soon will be) in service, we can consider using space imagery as another approach to monitoring marine mammals. Space Imaging, LLC, put the first of these new satellites, Ikonos, into orbit in late 1999. Ikonos' resolution is 1 m and 4 m in panchromatic (pan) and four multispectral (MS) bands, respectively. Prior to the deployment of Ikonos, the best available imagery was provided by Spot 4 (10 m and 20 m) and LANDSAT-7 (15 m and 30 m), resolutions insufficient for the detection of marine mammals.

The Ikonos, QuickBird, OrbView 3, and Spot 5 satellites are offering simultaneous imaging in pan and MS. The MS bands are similar to the first four LANDSAT bands, TM1 through TM4 (blue, green, red, and near IR). OrbView 4 will be a pan and hyperspectral system. EROS A1 has only a pan capability.

Table 1. Existing and planned commercial high-resolution satellites.

Vendor	Satellite	Pan/MS Resolution (m)	Service date
Space Imaging, LLC	Ikonos	1/4	9/1999
ImageSat International	EROS A1	1.8/NA	12/2000
EarthWatch Incorporated	QuickBird	0.6/2.4	9/2001 (est.)
OrbImage[a]	OrbView 3	1/4	2001, Q4
OrbImage	OrbView 4[b]	2/8	2001, Q4
Spot Image	Spot 5	2.5/10	2002

[a]OrbImage: Orbital Imaging Corporation.
[b]OrbView 4 is hyperspectral.

Satellite imagery offers several potential advantages. Satellites can obtain data more quickly and easily than aerial campaigns, especially in areas that are very far from aircraft bases of operation. The main cause of delay in a satellite survey is cloud cover, but when conditions are favorable, a satellite can survey 10,000 km^2 in one overpass, and the data can theoretically be processed and reduced to an animal census within 1 week. The same area would require several weeks to months to survey with aircraft. Also, a satellite's imagery collection can be scheduled for the optimum sunlight, weather, and sea-state conditions. The client pays for only the imagery collected

under specified conditions. The cost is competitive with that of aerial surveys. One Ikonos image, for example, covers 140 km^2 at a cost of \$1,700–\$4,000, depending on the location and tasking fees. Ikonos imagery is guaranteed to be 80% cloud free.

Satellite imagery also has its limitations. The two most important are resolution and quantization noise. The resolution of satellite imagery will continue to improve in future systems but is far from competitive with that of human vision from low-altitude aircraft. Quantization noise is a significant issue, because satellite imagers and the associated electronics are designed to cover radiance levels of land applications such as vegetation and urban infrastructures. Radiance from the ocean and marine subjects is usually far less than that from land features, and is limited to a few lowest-order bits of the image dynamic range. Thus, quantization noise could be a severe limitation.

Marine mammal detection in ocean scenes may also be affected by natural clutter such as that caused by surface waves.

The purpose of the short study reported here was to take an initial look at these issues and determine the feasibility of detecting marine mammals from satellite imagery. A simple signal and noise model was developed, and signal-to-noise ratios (SNR) were derived. Two types of signal detectors were modeled and evaluated. One type uses a matched filter on a single-image spectral band, which can be either pan (0.45–0.9 μm) or one of the MS bands. The second type of detector combines two spectral bands and exploits spectral differences between signal and noise. The advantage of panchromatic images is high resolution, which is better for the detection of smaller targets such as porpoises. On the other hand, MS images can reject more background clutter. This paper reports detection with the MS bands only. Pan and pan-MS fusion will be covered in a future paper.

II. SIGNAL MODEL

A. Signal Shape

The canonical signal used in this paper is an elliptical target of length L, and a 14:3 major/minor ratio. The ellipse orientation is variable. The dimensions correspond to those of a medium-size marine mammal. The target shape is outlined by $s_0(\underline{\boldsymbol{x}})$, $\underline{\boldsymbol{x}}$ = x,y image coordinates. The signal is then scaled to units of radiance by a model described below.

B. Radiance

As illustrated in Fig. 1, radiance at the sensor can be modeled as a sum of the following three components:

L_{path}—atmosphere path radiance
L_{sky}—fresnel surface reflection of skylight
L_{water}—water-leaving radiance.

We chose to ignore sun glint and whitecaps, to keep the model simple. We assume that precautions are taken to avoid sun glint and to edit whitecaps from the data. The operator can avoid sun glint by pointing the sensor at least 30^o from the sun specular angle. Pixels contaminated with whitecaps can be identified by their radiance and spectral characteristics. Such pixels are then flagged for exclusion from subsequent processing.

L_{water} can be broken down into two terms: $L_{vol,}$ for radiance from water volume scattering; and $L_{b,}$ for the radiance of the target. The total radiance at the sensor is then approximated, as in [4] and [5], by the following:

$$L_{sensor} = L_{path} + t\,[L_{sky} + L_{water}]$$

$$= L_{path} + t\,[L_{sky} + e^{-2\,a\,z} L_b + (1 - e^{-2\,a\,z}) L_{vol}] \quad , \qquad (1)$$

where t is the atmosphere transmission coefficient, a is the water attenuation coefficient, and z is depth. Everything except z depends on wavelength. The wavelength dependence is suppressed, for notational simplicity.

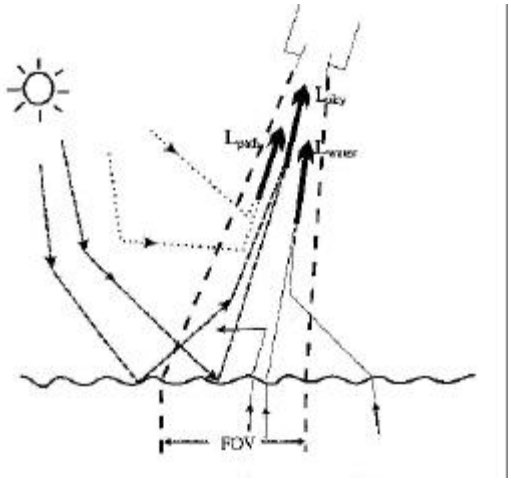

Source: Stuffle and Douglas [3]

Fig. 1. Ocean radiance model.

Equation (1) is used in bathymetry [3, 4], where L_b represents the radiance of the ocean bottom substrate. The equation can be inverted to derive bottom depth. Here we assume infinite ocean depth, so water-leaving radiance is

simply $t \cdot L_{vol}$ in all the pixels except those pixels with the additional target (marine-mammal) reflectivity, L_b.

In common practice, the area wide average values of L_{path} and L_{sky} are estimated by a model or model-data process and subtracted from the image radiances. The atmosphere-corrected signal is then

$$s(\underline{\boldsymbol{x}}) = s_0(\underline{\boldsymbol{x}}) \cdot L_{water} \cdot (x - 1) \cdot e^{-2\,a\,z} \quad , \qquad (2)$$

where x is the target's spectral reflectivity relative to the ocean background, or L_b/L_{water}. L_b is a target parameter. L_{water} can be estimated from the data. The term x is also the visual contrast of the target to surrounding ocean when the target is on the surface. For a completely black target, $x = 0$; the signal level is $-L_{water} \cdot e^{-2a\,z}$; and represent the blocking of upwelling light from depth below the target. In the $x > 1$ case, the target appears brighter than the ocean; in the $x < 1$ case, the target blocks more light than it reflects and appears darker than the ocean.

The special case $x = 1$ corresponds to a target with reflectivity that exactly matches the ocean. Such a target is optically stealthy.

C. Spectral Reflectivity

There are numerous sources of typical values for two terms in (2), L_{water} and a. But unfortunately there appear to be no sources of values for spectral reflectivity, and, more specifically, of values for the ratio x for marine mammals. Since an SNR prediction cannot be made without some estimate of x, we have used the RGB values from color photographs in the National Marine Mammals Laboratory photo gallery [6] and other resources on the Internet. For example, Fig. 2 shows a typical aerial photo from [6], Cetacean Photo Gallery 1. RGB values on the animal's surface were used for target radiance, and RGB values in the darkest water pixels were used for ocean radiance.

Fig. 2. Aerial photo of blue whale, used for rough estimate of spectral reflectivity.

Although these values are not radiometrically calibrated, the animal-to-ocean ratio is assumed to be a useful measure of the relative spectral reflectivity, x. Fig. 3 summarizes the relative reflectivity obtained by this procedure. The reader is cautioned that these values are very approximate and are provided only for initial SNR calculations in lieu of accurate spectral reflectivity. One interesting observation, however, can be made from the photo samples examined for this study: animal reflectivity is greater than water ($x > 1$) in all spectral bands.

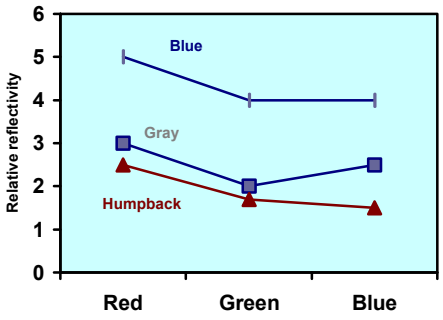

Fig. 3. Approximate spectral reflectivity, relative to deep water, for blue, gray, and humpback whales.

The photo method does not provide information on near-IR reflectivity. The near-IR reflectivity of animals is probably much higher than that of the surrounding water. If that is the case, near-IR reflectivity would be very useful for detecting animals on the ocean surface. However, we leave that question to be answered in a future study. The rest of this paper emphasizes detection just below the surface and deeper.

III. SNR LIMITED BY QUANTIZATION NOISE

There are several possible sources of noise: the spatial variability in L_{path} and L_{sky}, shot noise, sensor dark current, and quantization. We assume that L_{path} and L_{sky} are uniform. In some viewing angles, L_{sky} can be modulated by ocean wave slope. We will see (section V) that some L_{sky} variability noise can be removed by spectral processing. For the moment, however, we consider L_{sky} to be uniform and thus not a noise factor. In current systems, shot noise is well below the quantization level.

The "best case" SNR is based on the assumption that the only noise is quantization, or the randomness of the lowest-order bit. In that case the expected SNR is

$$ESNRQ = (2\,(A\,/DX^2)\,L_{water} \cdot (x - 1) \cdot e^{-2\,a\,z}) \,/\, DL \quad , \qquad (3)$$

where A is the target area in the image, DX^2 is the pixel area, and DL is water-leaving radiance per digital count, or, alternatively, sensor radiance per digital count / t.

Table 2 lists the sensor and spectral radiance parameters used in this paper. The values for water optical properties, L_{water} and $\mathfrak{G}$ are illustrative—the actual values vary widely with water type. The sensor bands are for Ikonos but are similar to those of other satellites. The *DL* values are for Ikonos.

Table 2. Sensor and radiometric parameters. Radiance levels are in units of mW/m^2 sr μm.

			Band	
Parameter	Near IR	Red	Green	Blue
Center μm	805	665	551	481
Width μm	102	70	95	76
ΔL	0.264	0.283	0.263	0.329
L_{path}	8.0	11.0	23.0	41.0
L_{sky}	0.18	0.32	0.56	0.74
L_{water}	0	0.48	2.5	3.1
τ	0.73	0.76	0.70	0.63
α	2.0	0.4	0.08	0.02

The canonical target on the ocean surface ($z = 0$) is easy to detect in all spectral bands. For example, using the gray whale spectral reflectivities in Fig. 3 with the parameters in Table 2, *ESNRQ* = 19, 28, and 31 dB for the red, green, and blue bands, respectively. A more complex task is the detection of a submerged target. Water quickly attenuates a signal in the near-IR and red bands, so that the signal is predominantly in the green-blue band if it is detected at all. In deep ocean the blue band has the greatest depth penetration. Fig. 4 plots the depth dependence of *ESNRQ* for the canonical target, with a conservative blue-band relative reflectivity of $x = 2$.

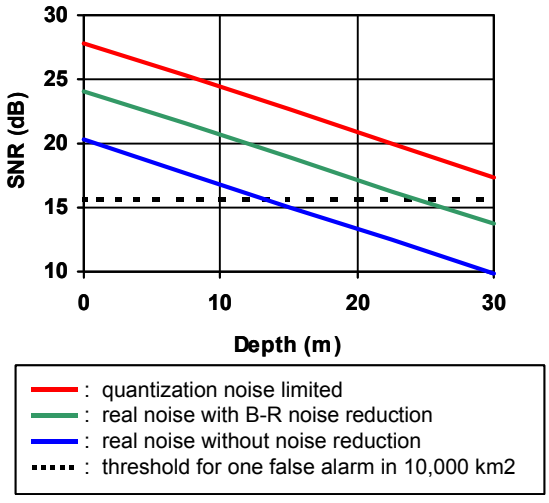

Fig 4. SNR vs. depth.

IV. SNR IN REAL DATA

A. Image Data

An Ikonos image of part of Roatan Island and an adjacent ocean area (centered at 16°.4 N 86°.6 E) is used as an example of real noise. The image was taken on 12 March 2000, 15:56:09 UT. The sun zenith angle was 35° at azimuth 122°. Fig. 5 shows the entire image.

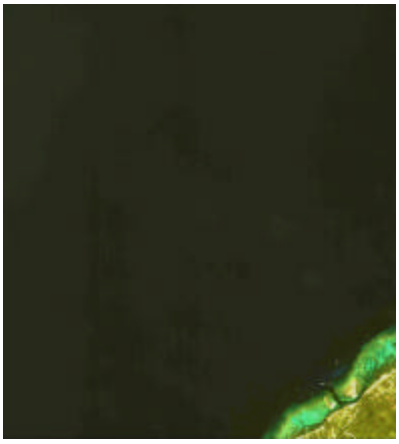

Source: Space Imaging, LLC.

Fig. 5. Roatan image.

The land mass at the lower right corner is a section of the north coast of Roatan. The figure also shows coral reefs just offshore and the wakes of several small vessels entering Bailey's Cay, shown enlarged in Fig. 6. Fig. 7 is a closeup view of the wakes of two boats, each about 60 m long. An average whale is 25% the size of these wakes.

These images are corrected for atmospheric effects. The original data has 11 bits. The ocean appears black because its radiance is 2% of that of the coral and land features and is represented in the lowest 4–5 bits.

Source: Space Imaging, LLC.

Fig. 6. Closeup of Bailey's Cay.

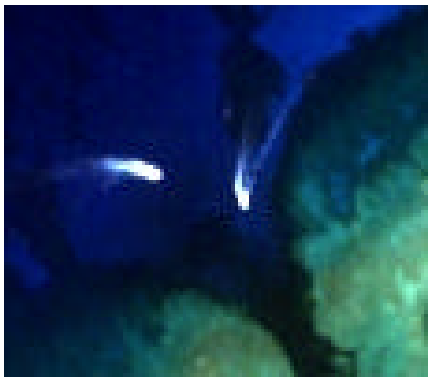

Source: Space Imaging, LLC.

Fig. 7. Closeup of boat wakes.

B. Noise Power Spectrum

A deep-water area in the upper left corner of the full image (Fig. 5) was used as a sample of real ocean data for the further analysis that follows. In Fig. 8 the color image intensities were equalized to better show the spatial structure of the ocean surface.

All the spatial structure apparent in Fig. 8 spans a very narrow range of radiance levels. The standard deviation is 0.37 mW/m^2 sr μm, which is only slightly more than the 1-bit resolution, but the noise is clearly more complex than quantization noise. The dark strip in the middle is probably a sensor artifact. Ocean waves with crests aligned approximately vertically are also evident. The power spectrum of the image (Fig. 9) shows the wave spectrum more clearly. The predominant wavelength is 50 m. At Nyquist (0.125 c/m) the spectral power has dropped to a level about twice that predicted for quantization noise.

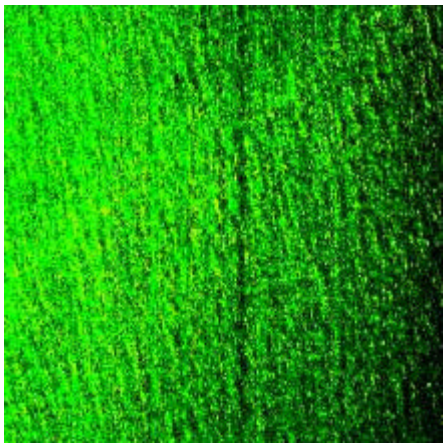

Fig. 8. Deep water area.

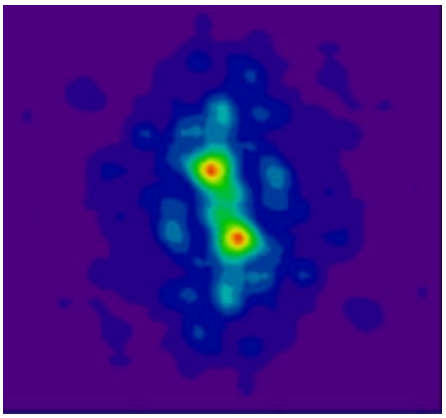

Fig. 9. Power spectrum of deep water area.

C. Matched-Filter Detector

The above spectrum analysis shows that the real noise is nonwhite. The optimum detector in that case is a correlator of the data (d) with the signal (s) normalized by the noise covariance matrix (K), otherwise known as the matched filter. In notation similar to that used in [7] the detector output is

$$V = d^T K^{-1} s \quad , \tag{4}$$

and the expected SNR ($ESNR$) is

$$\begin{aligned} ESNR &= \mathrm{E}[V x \mathrm{H}_1] \\ &= \mathrm{var}[V x \mathrm{H}_0] = \int S(\underline{\boldsymbol{k}})/N(\underline{\boldsymbol{k}})\, \mathrm{d}\underline{\boldsymbol{k}} \quad , \end{aligned} \tag{5}$$

where V is the detector output under either the H_0 (null hypothesis) or H_1 (signal present) hypothesis; S and N are the power spectra of, respectively, the signal and noise, in the wave number ($\underline{\boldsymbol{k}}$) domain.

The spectrum of the signal spans a range of wavenumbers. The matched filter will down-weight the signal wavenumbers where the noise spectrum is high and emphasize those where the noise is lower.

As (5) implies, there are three ways of computing expected ESNR: first, by injecting a signal into the image and measuring the detector peak output, V; second, from the variance of the detector output in the absence of a signal; and third, by integrating S/N over the signal wave number support. All three methods are statistically identical; the easiest, S/N integration, is used here.

The $ESNR$ in the Roatan image can be compared to the baseline $ESNRQ$ in Fig. 4. $ESNR$ is slightly dependent on the target orientation with respect to the surface waves. The values used in Fig. 4 are averaged over all orientations. It can be seen that detections in the real data fall 8 dB short of quantization-limited $ESNRQ$. This result is not

surprising, since the effect of the noise is to down-weight a significant fraction of signal energy in the lower wave-number regions, i.e., in the wavenumbers with ocean wave noise.

Presumably such degradation can be avoided by choosing more favorable data collection conditions, i.e., either by using a sensor viewing angle that minimizes ocean wave visibility or by choosing a day with calmer sea. In the next section we show another way to avoid degradation.

V. SNR WITH NOISE REDUCTION

Presumably, the dominant noise in the Roatan image (Fig. 5) is related to the wave-slope modulation of L_{sky}. This modulation should be correlated between all spectral bands. There are several sophisticated methods of exploiting such correlations to increase SNR. For purposes of illustration, we will use the simple B-R method, which coherently subtracts red from blue. This method works if the red band contains only the noise and the blue band contains signal plus noise. This assumption is reasonable in this application, since the red channel contains signal only when the target is on or very near the surface. In that case the SNR is already very high and noise cancellation is not needed. At greater depths, where noise cancellation is critical, the red band signal is greatly attenuated and the red channel can be used as a reference for noise cancellation.

The B-R method is implemented by first subtracting the correlated noise in R from the B band and than applying the matched filter as before.

In the Roatan case, B-R reduced the spectral power of the 50 m waves by a factor of 10. Some nonwhite noise remained, but ESNR improved substantially. As shown in Fig. 4, the simple noise cancellation improved SNR by 4 dB and left only a 4 dB gap with respect to *ESNRQ*.

VI. DETECTION THRESHOLD

A threshold must be applied to detector outputs to avoid false alarms, e.g., identifying a random noise occurrence as a marine mammal. For normally distributed detector output, a threshold for one false alarm in N_0 detector outputs is

$$T = 10 \log(2 \cdot \ln (N_0/ (2\pi)^{1/2})) \text{ dB} \quad (6)$$

[8]. The detection threshold in Fig. 4 (shown as a broken line) corresponds to one false alarm per 10^4 km^2. At this threshold a canonical target can be detected in the blue band to a depth of 12 m. Using the B-R method increases maximum detection depth to 24 m.

The actual detection depth limit depends on the target size and reflectivity. The maximum depth for a humpback whale is 10 m because of its lower blue reflectivity. On the other hand, the size and reflectivity of a blue whale increases SNR by 12 dB and increases detection depth to 50 m.

VII. SUMMARY AND CONCLUSIONS

The signal and noise model and related SNR calculations presented here support the idea of using satellite imagery to monitor marine mammals. Satellites might now take over some of the surveys currently accomplished with aerial transects.

We must, however, stress that the SNR calculations are based on crude estimates of target spectral reflectivity. A library of accurate spectral reflectivity data for marine mammals would significantly increase confidence in the SNR prediction. Spectral reflectivity data are also needed to implement an optimum multiband detection algorithm. Finally, accurate data on spectral reflectance properties might be important for discriminating real targets from false alarms, e.g., whitecaps.

Satellite imagery will not entirely replace aerial surveys. Aerial observers still have significantly greater resolution, which is critical for identifying smaller animals and differentiating species. Some aerial studies track individual animals, a feat beyond current satellite resolution. The aerial-survey advantage will, however, narrow when commercial satellites double their resolution as planned in the near future.

Pan-MS fusion, another mechanism for higher resolution, combines the benefits of higher resolution in the pan image with MS clutter noise cancellation. Results obtained with a pan-MS fusion algorithm will be described in a future paper.

Satellite imagery also could be improved by enhanced noise cancellation. This paper shows performance within 4 dB of the limit set by quantization noise with a simple noise cancellation algorithm. It would be interesting to investigate more sophisticated techniques and eliminate the remaining noise.

The most important improvement that could be made in marine mammal detection is to lower the minimum detectable radiance (i.e., to lower *DL*). Other marine applications such as bathymetry, navigation hazards detection, water turbidity measurements, and water pollution monitoring will also benefit. Unfortunately, this improvement is not a near-term prospect, since it requires the redesign of the imaging sensor.

Acknowledgments

The author is grateful to Ms. Tish Williams and Mr. Dave Ward of Space Imaging, LLC, for their assistance and support. Space Imaging provided the Ikonos image for this study.

REFERENCES

[1] J.V. Carretta, M.S. Lowry, C.E. Stinchcomb, M.S. Lynn, and R.E. Cosgrove, *Distribution and Abundance of Marine Mammals at San Clemente Island and Surrounding Offshore Waters: Results from Aerial and Ground Surveys in 1998 and 1999*, NOAA, National Marine Fisheries Service Administrative Report LJ-00-02, April 2000.

[2] J.R. Mobley, Jr., P.H. Forestell, R. Grotefendt, E.K. Brown, A. Bowles, T. Norris, and M. Smultea**,** "Aerial surveys of humpback whales wintering in Hawaiian waters: 1993 results," Tenth Biennial Conference on the Biology of Marine Mammals, Galveston, Texas, November 1993.

[3] L.D. Stuffle, *Bathymetry from hyperspectral imagery*, master's thesis, Naval Postgraduate School, December 1996.

[4] P.N. Bierwirth, T. Lee, and R.V. Burne, "Shallow sea-floor reflectance and water depth derived by unmixing multispectral imagery," *Photogrammetric Engineering and Remote Sensing*, Vol. 59, No. 3, pp. 331–338, 1993.

[5] D.L.B. Jupp, "Background and extensions to depth of penetration (DOP) mapping in shallow coastal waters," Symposium on Remote Sensing of the Coastal Zone, Gold Coast, Queensland, 1988.

[6] NOAA, "Cetacean Photo Gallery 1," http://nmml.afsc.noaa.gov/gallery/cetaceans.htm, National Marine Mammal Laboratory, National Oceanic and Atmospheric Administration, November 2000.

[7] H. Urkowitz, *Signal Theory and Random Processes*, Dedham, MA: Artech House, 1983, section 15-2.2.

[8] E.J. Gumbel, *Statistics of Extremes*, New York: Columbia University Press, 1958, p. 139.